The influence of precipitation variability and partial irrigation within grid cells on a hydrological simulation

Qiuhong Tang[*] and **Taikan Oki**[†]

Institute of Industrial Science, University of Tokyo, Tokyo 153-8505, Japan

Shinjiro Kanae[‡]

Research Institute for Humanity and Nature, 335 Takashima-cho, Kamigyo-ku,

Kyoto 602-0878, Japan

Heping Hu[§]

Institute of Hydrology & Water Resource, Tsinghua University,

Beijing 100084, China

October 17, 2006

[*]Corresponding author. Tel: +81-3-5452-6381 Fax: +81-3-5452-6383 Email: tangqh@iis.u-tokyo.ac.jp
[†]Tel: +81-3-5452-6381 Fax: +81-3-5452-6383 Email: taikan@iis.u-tokyo.ac.jp
[‡]Tel: +81-75-229-6180 Fax: +81-75-229-6150 Email: kanae@chikyu.ac.jp
[§]Tel: +86-10-6278-2356 Fax: +86-10-6278-5699 Email: huhp@tsinghua.edu.cn

Abstract

We evaluated the effects of natural and anthropogenic heterogeneity on a hydrological simulation using a distributed biosphere hydrological model (DBHM) system. The DBHM embeds a biosphere model into a distributed hydrological scheme, representing both topography and vegetation in a mesoscale hydrological simulation, and the model system includes an irrigation scheme. We investigated the effects of two kinds of variability, precipitation variability and the variability of irrigation redistributing runoff, representing natural and anthropogenic heterogeneity, respectively, on hydrological processes. Runoff was underestimated if rainfall was placed spatially uniformly over large grid cells. Accounting for precipitation heterogeneity improved the runoff simulation. However, the negative runoff contribution, namely the situation that mean annual precipitation is less than evapotranspiration cannot be simulated by only considering the natural heterogeneity. This constructive model shortcoming can be eliminated by accounting for anthropogenic heterogeneity caused by irrigation water withdrawals. Irrigation leads to increased evapotranspiration and decreased runoff, and surface soil moisture in irrigated areas increases because of irrigation. Simulations performed for the Yellow River basin of China indicated stream flow decreases of 41% due to irrigation effects. The latent heat flux in the peak irrigation season (June, July, August: JJA) increased 3.3 W m^{-2} with a decrease in the ground surface temperature of 0.1 K for the river basin. The maximum simulated increase in the latent heat flux was 43 W m^{-2}, and the ground temperature decrease was 1.6 K in the peak irrigation season.

1. Introduction

The land surface-atmosphere interface is a major component of the climate system, characterized by hydrologic coupling between the atmosphere and the land biosphere. Several land surface models have been developed to describe land-atmosphere water and energy exchanges, including the bucket model (Manabe 1969), Biosphere-Atmosphere Transfer Scheme (BATS) (Dickinson et al. 1986), the Simple Biosphere (SiB) model (Sellers et al. 1986), and the Bare Essentials of Surface Transfer (BEST) (Desborough and Pitman 1998). These models emphasize the vertical structure, representing the land surface as one or two tiers of vegetation (i.e., canopy or groundcover, or both). However, one of the main shortcomings of these schemes is that they do not capture the pronounced heterogeneity of the Earth's land surface. This heterogeneity spans a wide range of scales and affects the surface energy and water budgets, as well as land-atmosphere exchanges of momentum, heat, and water through several nonlinear processes. Distributed representations of spatial information and physical descriptions of the land biosphere and hydrological processes are necessary because of their spatial heterogeneity and highly nonlinear form. The resolution of present-day general circulation models (GCMs) is still too coarse to explicitly capture the effects of surface heterogeneity, which must thus be parameterized within the framework of complex and nonlinear land surface process schemes. A realistic representation of subgrid-scale variability would markedly improve land surface modeling (Koster and Suarez 1992a).

Numerous studies have investigated the subgrid-scale variability associated with terrain, soil, and vegetation heterogeneities. Milly and Eagleson (1988) found that surface runoff could be greatly underestimated if the areal variability of precipitation associated with various scales and types of storms were ignored. Entekhabi and Eagleson (1989) used analytic distributions of rainfall and soil moisture conditions to examine the sensitivity of runoff, bare soil evaporation efficiency,

and transpiration efficiency to soil type and climatic forcing. Avissar and Pielke (1989) suggested a parameterization of subgrid-scale forcing for heterogeneous land surfaces in atmospheric numerical models and found that spatial heterogeneity in vegetation could have significant effects on temperature and precipitation. Pitman et al. (1990) used a surface hydrology model driven by meteorology simulated by a GCM to investigate the influence of the subgrid distribution of precipitation on the surface water balance. Their results indicated that improving the realism of the areal distribution of precipitation could alter the partitioning between runoff and evapotranspiration. Seth et al. (1994) divided one GCM grid into several subgrids to study the effects of subgrid-scale vegetation and climate specifications on surface fluxes and hydrology, and showed that energy partitioning at the surface, surface stress, and runoff could all be significantly affected by subgrid variability. Ghan et al. (1997) presented a preliminary evaluation of the relative importance of subgrid variations in parameters related to the surface hydrology. They found that subgrid variability in summertime precipitation would increase runoff, and subgrid variations in vegetation and soil properties would increase surface runoff and reduce evapotranspiration. Giorgi (1997a,b) described a theoretical framework for the representation of surface heterogeneity within complex biophysical surface schemes for use in climate models and assessed the sensitivity to relevant parameters.

Giorgi and Avissar (1997) reviewed methodologies for the representation of land surface subgrid-scale heterogeneity effects and grouped the effects of surface heterogeneity into two categories: ”aggregation” and ”dynamical” effects. Subgrid-scale aggregation has been shown to affect the simulated surface latent and sensible heat fluxes, snowpack, and dynamics of soil moisture and runoff. Dynamical heterogeneity effects are associated with microscale and mesoscale circulations induced by heterogeneous surfaces. Models of dynamical heterogeneity processes attempt

to describe the effects of atmospheric circulations induced by surface heterogeneities (Seth and Giorgi 1996; Avissar and Schmidt 1998). Models of aggregation effects attempt to calculate the contribution of different subgrid-scale surface types to the grid box average energy and water budgets and surface-atmosphere exchanges. Such models have been based on discrete approaches, whereby heterogeneity is described in terms of a finite number of subgrid ”tiles” or ”patches,” and on continuous approaches, in which heterogeneity is described in terms of probability density functions. Many researchers have used probability density functions within continuous approaches to investigate the variability of precipitation and soil characteristics (Entekhabi and Eagleson 1989; Gao and Sorooshian 1994; Liang and Xie 2001; Zeng et al. 2002; Yeh and Eltahir 2005). Several studies have also represented land use and vegetation cover subgrid variability based on discrete approaches (Koster and Suarez 1992b; Leung and Ghan 1998). Koster and Suarez (1992b) considered two conceptually different strategies, the ”mixture” and ”mosaic” strategies, for dealing with subgrid variability in vegetation cover. The mixture strategy assumes that the different vegetation types are effectively mixed homogeneously throughout the grid square, so that the atmosphere interacts only with a set of near-surface atmospheric conditions pertaining to the mixture. With the mosaic strategy, the different vegetation types in a grid square are assumed to be geographically distinct. The different types are viewed as separate tiles of a square grid mosaic, and each tile interacts with the atmosphere independently. The effective differences between the strategies are small over a wide range of the condition. In particular, the strategies are effectively equivalent when the transpiration resistances of the different vegetation types are of the same order of magnitude.

Although the subgrid variability of natural factors, such as precipitation, soil infiltration capacity, and vegetation cover, has been extensively studied, few studies have investigated the subgrid-scale variability caused by human activities. Döll and Siebert (2002) modeled the global irrigation

water requirements under present-day climate conditions and found that the annual irrigation water requirement in hot semiarid regions can be more than 1000 mm. Boucher et al. (2004) concluded that human activity through irrigation has a direct influence on the water vapor concentration, and estimated a global mean radiative forcing up to 0.1 W m^{-2} and a surface cooling of up to 0.8 K over an irrigated area. Gordon et al. (2005) showed that deforestation is as large a driving force as irrigation in terms of changes to the hydrological cycle. Haddeland et al. (2005) reported on an irrigation scheme in a macroscale hydrological simulation and evaluated the effects of irrigation on the water and energy balances of the Colorado and Mekong river basins. These studies indicated that the subgrid variability caused by human activities has potentially important effects on the surface water and energy balances. However, few complete studies have described the effects of both the subgrid variability of natural factors and human activities on hydrological simulation. In particular, few studies have examined the influence of subgrid variability on large-scale distributed hydrological patterns within a large river basin.

Among the subgrid heterogeneities affecting hydrological processes, we account for two heterogeneities: precipitation heterogeneity and the heterogeneity of irrigation redistributing runoff; these factors represent the natural subgrid variability and the variability caused by human activities, respectively. Precipitation heterogeneity is represented by a simple spatial exponential distribution. An irrigation scheme based on simulated soil moisture and available water was developed to represent subgrid variability related to irrigation. The study objective was to analyze the effects of anthropogenic heterogeneity on the water and energy balances of a large-scale basin in a semiarid river basin by comparing the effects of natural heterogeneity and anthropogenic heterogeneity.

2. Model description

A modeling framework was developed to represent the effects of natural and anthropogenic heterogeneity on the water and energy balances of a large river basin. The modeling framework, a distributed biosphere hydrological model (DBHM), embeds a biosphere model into a distributed hydrological scheme, representing both topography and vegetation conditions in a mesoscale hydrological simulation (Tang et al. 2006).

In the DBHM system, the revised Simple Biosphere (SiB2) model (Sellers et al. 1996) is used to calculate the transfer of energy, mass, and momentum between the atmosphere and the surface of the Earth, and a river routing scheme is used to lead the runoff to the river basin outlet. The overall structure of DBHM system is shown in Fig. 1.

[Figure 1 about here.]

The Food and Agriculture Organization (FAO) Digital Soil Map of the World (FAO 1995) was used to produce the DBHM grid soil properties, such as the soil water potential at saturation ψ_s (m), soil hydraulic conductivity at saturation K_s (m/s), soil wetness parameter b, and porosity θ_s (Cosby et al. 1984).

The surface overland flow is described by the one-dimensional kinematic wave model that includes the continuity equation (Lighthill and Whitham 1955; Hager 1984):

$$\frac{\partial h_s}{\partial t} + \frac{\partial q_s}{\partial x} = i \tag{1}$$

and momentum equation:

$$q_s = \frac{1}{n} S_0^{1/2} h_s^{5/3} \tag{2}$$

where h_s is the surface overland flow depth (m), q_s is the overland discharge per unit width (m^2/s), t is time (s), x is the distance along the overland flow (m), i is surface runoff in water depth (m), S_0 is the friction slope gradient, and n is Manning's roughness parameter.

The flow between the river network and the groundwater is considered to be groundwater flow to a ditch over a sloping impermeable bed (Childs 1971; Towner 1975). Assuming that the flow lines are approximately parallel to the bed, according to the Dupuit-Forchheimer approximation, the flow of water per unit width of the river can be written in terms of the hydraulic conductivity and the absolute slope of the water table:

$$q_g = K_s h_g \left[\frac{dh_g}{ds} \cos\theta + \sin\theta \right] \tag{3}$$

where q_g is the flow between the groundwater and river water (m^2/s), θ is the bed slope (rad.), s is the distance along the riverbed (m), and h_g is the aquifer thickness (m). If q_g is positive, it is base flow for water-gaining streams. If q_g is negative, it is river recharge for water-losing streams.

The river flow is governed by the following continuity equation (Lighthill and Whitham 1955; Chow 1959):

$$\frac{\partial Q}{\partial x} + \frac{\partial (B \cdot h)}{\partial t} = q_s + q_g \tag{4}$$

and momentum equation:

$$Q = \frac{1}{n(B+2h)^{2/3}} S_r^{1/2} (B \cdot h)^{5/3} \tag{5}$$

where Q is the river discharge (m^3/s), B is the river width (m), h is the flow depth (m), and S_r is the riverbed slope. Estimation of the Manning's roughness parameter n for natural streams was based on field observations guided by Chow (1959) and Acrement and Schneider (1989). In this study, n = 0.12.

This section describes the modification of the SiB2 model to include a river-routing module and an irrigation scheme.

2a. *SiB2 and river-routing module*

The SiB2 model is grid-based and designed for use in atmospheric general circulation models. It calculates the water and energy balance equations at the land surface. In the SiB2 model, precipitation consists of large-scale spatially uniform precipitation and convective spatially nonuniform precipitation. In most GCMs, a single (area-averaged) figure for convective precipitation is produced for each grid area for each time step. The SiB2 model can use GCM outputs of large-scale and convective precipitation. In this study, we evaluated the relative importance of subgrid variations in precipitation and in human activities. Observations were used to drive a physically based model of the land surface water and energy balances. We assumed that the observed rainfall was spatially distributed according to a simple exponential $I(x)$:

$$I(x) = ae^{-bx} + c \tag{6}$$

where $I(x)$ is the relative amount of rainfall as a function of the fractional area of the grid area x, ($0 < x < 1$), and a, b, and c are constants (Figure 2). The constants a, b, and c are normalized so that the integration of $I(x)$ over the whole grid is 1. If set $a = b$, then $c = e^a$. The precipitation variability within grid cell will become large along with the increase of the value of parameters a. Sensitivity studies have been done on the parameters of the precipitation area-amount relationship. The runoff will increase along with the increase of the value of parameters a. The results are consistent with many similar studies on the effects of subgrid heterogeneity in precipitation

(Liang et al. 1996; Zeng et al. 2002). The precipitation parameters are important and can vary largely with time. It is more realistic to obtain a good estimate of precipitation parameters for each storm based on radar images or other methods. However, more runoff will be generated in hydrological simulations with consideration of precipitation variability. For the long term simulation, the mean precipitation parameters can calibrated with the simulated and observed discharge in the river basin without human disturbance. For example, the headwater before the Tangnaihai station is lesser disturbed by human activities, and the discharge at the station was used to calibrate the precipitation heterogeneity parameters a, b, and c in equation 6. For cases accounting for precipitation heterogeneity before the Tangnaihai station, $a = b = 4$ was used.

[Figure 2 about here.]

Surface runoff and subsurface runoff were routed to the basin outlet through a channel network as described by Tang et al. (2006). The river basin and river network were abstracted from a 10-km digital elevation model (DEM). The Pfafstetter numbering scheme for delineation and codification of the river basin was used and based on topographic controls and the river network topography. The system was founded on concepts first described by Pfafstetter (1989) and later detailed by Verdin and Verdin (1999). The numbering scheme was self-replicating, making it possible to provide identification numbers to the level of the smallest subbasins from which four tributaries can no longer extracted from the DEM Verdin and Verdin (1999). The routing order of the subbasins was indicated in the Pfafstetter code. Within a given smallest subbasin, flow intervals were specified to represent the time lag and accumulating processes in the river network according to the distance to the subbasin outlet. The surface runoff flowed to the river channel following a hillslope, as governed by a one-dimensional kinematics wave model. The subsurface runoff connected the river channel to a groundwater reservoir. The river flow was governed by a kinematics wave model,

taking into account the friction of the river channel.

The input data to the SiB2 model were hourly precipitation, temperature, vapor pressure, wind speed, shortwave downward radiation, and incoming longwave radiation. When the hourly input data were not supplied to the model, we partitioned these variables in the model time step based on daily precipitation and maximum and minimum temperatures, using standard algorithms or empirical relationships (Cesaraccio et al. 2001). The vapor pressure was estimated from observed relative humidity and temperature (Allen et al. 1998). The downward shortwave radiation was estimated from sunshine duration. Because elvation of the upper stream of Yellow Riverbasin is very high, the widely-used FAO Angström-type model (Angström 1924; Doorenbos and Pruitt 1977) may under-estimate shortwave radiation. Therefore, we adopted a new and widely validated radiation model (Yang et al. 2001; Yang and Koike 2005) to estimate the radiation, with hourly sunshine data interpolated from daily data following Revfeim (1997). The daily wind speed was directly used as hourly wind speed.

2b. *Irrigation scheme*

In each grid cell, land use was partitioned into an irrigation part and nonirrigation part, based on the Global Map of Irrigated Areas (Siebert et al. 2005) dataset. The irrigation part of the land use was set as the SiB2 land use of ”Agriculture or C3 Grassland.” The nonirrigation part was obtained from the Global Land Cover Characterization dataset (Loveland et al. 2000). For the calculation of water and energy fluxes between the atmosphere and land surface, the mosaic strategy was used. The SiB2 model was performed at irrigation and nonirrigation tiles, respectively, and each tile interacted with the atmosphere independently. The runoff from irrigation and nonirrigation tiles was mixed homogeneously throughout the grid square and routed to the river channel.

The irrigation scheme was based on simulated soil moisture in the irrigation tiles and available water for irrigation. The main purpose of irrigation was to keep the soil moisture in the irrigation tiles above the wilting point level. The SiB2 model was modified to consider irrigation water use, based on the predicted soil moisture. Irrigation started when the soil moisture was below the wilting point level and continued until soil moisture reached the field capacity level. During the irrigation time, if precipitation charged the soil water and soil moisture reached the field capacity level, irrigation would stop. The water loss in the irrigation channel was not considered in this approach, so the simulated irrigation requirement was the net irrigation consumption. The irrigation water requirement is defined as the estimated irrigation requirement if there is no limitation of water supply. The available water for irrigation was estimated based on the predicted river flow by the river routing module. Irrigation water can be extracted from two possible sources, local river runoff or river runoff at an assigned river channel. Basically, the irrigation water was extracted from river runoff locally. For the central irrigation area, the grid clusters were recognized as irrigation districts. Irrigation districts usually extract irrigation water from specific river channels. If an irrigation district is outside the river basin, the irrigation water is taken from specific river channels, usually the nearest main stem of the river network for a water supply that is as steady as possible. No reservoir operation was taken into account in this study, although irrigation water availability might be affected by reservoir management. Considering this realistic situation, the irrigation water withdrawal capacity was set for each water diversion gap.

3. Approach

3a. *Study area*

The model was applied to the Yellow River basin of China. The Yellow River is the second-longest river in China. The headwaters of the Yellow River begin on the Tibetan Plateau, and the river flows eastward, passing though the Loess Plateau and the North China Plain before emptying into Bohai Gulf (Figure 3). The main course of the river flows 5,464 km, and the river basin area is 794,712 km^2. The Yellow River faces serious water problems, including water shortages and eco-environmental degradation (Xu et al. 2002; Feng et al. 2005). In particular, the lower Yellow River has suffered from a drying-up phenomenon since the 1970s, and many researchers have focused on the river's hydrology (Liu and Zheng 2004; Fu et al. 2004; Xia et al. 2004; Yang et al. 2004; Xu 2005).

There are several irrigation districts inside the river basin, such as the Qingtongxia and Hetao districts (Figure 3). Some large irrigation districts in the lower reaches are located outside the watershed but extract irrigation water from the Yellow River (Fu et al. 2004; Chen et al. 2002). Liu and Zhang (2002) have described the status of irrigation in the river basin.

To validate the model and analyze the impact of subgrid-scale variability on stream flow, we examined the discharges from the following eight major hydrologic gauges on the main stream of the Yellow River: Tangnaihai (TNH), Lanzhou (LZ), Qingtongxia (QTX), Toudaoguai (TDG), Longmen (LM), Sanmenxia (SMX), Huayuankou (HYK), and Lijin (LJ) stations (Figure 3). The watershed above Tangnaihai station is the source region of the Yellow River, and water withdrawals from the river are limited. Qingtongxia station is downstream from a large irrigation district (the Qingtongxia irrigation district). Toudaoguai station is downstream from another large irrigation

district (the Hetao irrigation district). The Lanzhou-Qingtongxia and Qingtongxia-Toudaoguai sections are ”net” water consumption zones of the Yellow River, i.e., the annual discharge at Qingtongxia station is less than that at Lanzhou station, and the discharge at Toudaoguai station is less than that at Qingtongxia station. Huayuankou station is another key station on the main stream. The annual discharge at this station reaches the maximum value for the main river stem. Lijin is the last hydrological station before the river empties into Baohai Gulf. Between Huayuankou and Lijin stations, the runoff into the river channel is small because the elevation of the riverbed is higher than the land surface behind artificial levees. In addition, there are large irrigation districts in the lower reaches that are located outside the watershed and channeled river water (Fu et al. 2004; Chen et al. 2002). This area is another ”net” water consumption zone of the Yellow River.

[Figure 3 about here.]

3b. *Input data*

Climate data from 120 meteorological stations inside and close to the study basin (Figure 3) were obtained from the China Meteorological Administration (CMA). The dataset is available from 1983 to 2000 and contains the daily precipitation, mean temperature, maximum and minimum temperatures, mean surface relative humidity, sunshine duration, and cloud amount. The vegetation condition index leaf area index (LAI) and fraction of photosynthetically active radiation absorbed by the green vegetation canopy (FPAR) were obtained from Myneni et al. (1997). The LAI and FPAR datasets are available at monthly temporal frequencies from 1983 to 2000. Information about the percentage of irrigated area within each grid cell was obtained from Siebert et al. (2005). The meteorological data at the stations were interpolated to a 10×10-km gridded dataset using the angular distance weighted (ADW) averaging method (New et al. 2000). Figure 4 shows the mean

annual precipitation within a 10×10-km grid cell from 1983 to 2000, and also the percentage of irrigated area within the grid cells.

[Figure 4 about here.]

The LAI and FPAR datasets were resampled to the same resolution for use in the model. SiB2 land cover data are available from the USGS Global Land Cover Characterization dataset. The FAO Digital Soil Map of the World was used to produce the grid soil properties such as the soil water potential at saturation, soil hydraulic conductivity at saturation, soil wetness parameter, porosity.

4. Model validation

The model was tested for the Yellow River basin for the period from 1983 to 2000 after initializing the model until equilibrium was reached. Initially the model was run without considering the precipitation subgrid-scale variability and the irrigation scheme. There are no large irrigation districts near the upstream Tangnaihai station. The discharge observations at Tangnaihai station were considered to be the natural flow and were compared with the simulated stream flow. The mean bias (BIAS), root mean square error (RMSE), relative root mean square error (RRMSE), and mean square skill score (MSSS) were used to evaluate the model performance. The BIAS is defined as

$$BIAS = \frac{1}{N}\sum (x_s - x_o)/\overline{x_o} \tag{7}$$

where $\overline{x_o} = \sum x_o/N$ is the averaged value, RMSE is defined as

$$RMSE = \sqrt{\frac{1}{N}\sum (x_s - x_o)^2} \tag{8}$$

RRMSE is defined as

$$RRMSE = RMSE/\left(\sum x_o/N\right) \tag{9}$$

and MSSS is defined as (Murphy 1988)

$$MSSS = 1 - \frac{\sum \left(x_s - x_o\right)^2}{\sum \left(x_o - \sum x_o/N\right)^2} \tag{10}$$

where N is the total number of time series for comparison, x_s represents the simulated value, and x_o is the observed value. A perfect fit should have MSSS value equal to one. Mean monthly simulated and observed stream flow values from 1983 to 2000 are shown in Figure 5. The BIAS, RRMSE, and MSSS were 4.5%, 0.26, and 0.840, respectively. The simulated and observed daily stream flow at Tangnaihai station is shown in Figure 6. The RRMSE was 0.5, and the MSSS was 0.685. Monthly and daily discharge values were satisfactorily reproduced, and the discharge simulation performed reasonably well for estimating irrigation water availability.

[Figure 5 about here.]

[Figure 6 about here.]

For validation purposes, we implemented an irrigation scheme and compared the model-estimated net irrigation water consumption to the statistical water consumption from several previous reports. Liu and Zhang (2002) reported the water consumption in the upper, middle, and lower reaches of the Yellow River basin from the 1950s to 1990s; these values may be larger than the irrigation water consumption because the statistical water consumption included industrial and residential use. Li et al. (2004) provided the net irrigation water consumption in seven irrigation districts in the upper and middle reaches of the Yellow River basin. Table 1 lists the simulated and reported irrigation

water consumption. The reported numbers are summarized for the 1980s and 1990s, while the simulation results are averages for the corresponding periods. The simulated water consumption values in the upper reaches are less than reported values because large amounts of water are taken into the Hetao irrigation district, where water then drains to an endoric lake and evaporates into the atmosphere (Li et al. 2004).

[Table 1 about here.]

5. Analyses and Results

Model analyses were performed for a variety of modeling cases associated with natural and anthropogenic heterogeneities: case 1, no irrigation without consideration of precipitation heterogeneity; case 2, no irrigation with precipitation heterogeneity; case 3, irrigation with precipitation heterogeneity. For all the modeling cases, the same SiB2 land cover data from the USGS Global Land Cover Characterization dataset were used, along with the same vegetation characteristics, such as LAI and FPAR, and related soil optical properties. Possible vegetation status variety because of irrigation was not accounted for in the model.

Table 2 summarizes the effects of precipitation and anthropogenic subgrid variability on the mean annual water balance components of the Yellow River basin from 1983 to 2000. Without considering precipitation heterogeneity, the runoff contribution was underestimated for upper reaches. The simulated runoff contributions were less than observed contributions in the mountainous subdivision Up TNH. The simulations of runoff contribution were better by considering precipitation heterogeneity. The runoff contributions were always positive values in the cases without an irrigation scheme. This result contradicts the observed negative runoff contributions in arid regions, such as for subdivisions LZ-QTX and QTX-TDG. These results suggest that the negative runoff

contribution cannot be simulated by only considering the natural heterogeneity. This constructive model shortcoming can be eliminated by taking anthropogenic heterogeneity into account. With an irrigation scheme, the simulated annual runoff contributions in subdivisions LZ-QTX and QTX-TDG were -63 mm and -23 mm, corresponding to the observed contributions of -61 mm and -56 mm, respectively. The negative runoff contribution was modeled with the irrigation scheme. This result also indicates that irrigation water withdrawals have changed the pattern of the hydrological cycle in the Yellow River basin.

[Table 2 about here.]

Figure 7 shows the effects of precipitation heterogeneity on total runoff and subsurface runoff simulations from 1983 to 2000. The simulated total runoff for case 1 in which precipitation was spatially uniform over a large grid cell was much less than that of case 2 in which the precipitation heterogeneity was considered. The annual total runoff was 81 mm for case 1 and 101 mm for case 2. The simulated total runoff differences were caused by the surface runoff differences. The annual surface runoff was 20 mm and 43 mm for cases 1 and 2, respectively. This result indicates that surface runoff simulations highly depend on precipitation heterogeneity.

Figure 8 shows the effects of precipitation heterogeneity and irrigation on annual stream flow along the Yellow River from upstream to downstream. Compared to the case of no irrigation with precipitation heterogeneity (Case 2), discharge was underestimated for the case of no irrigation without precipitation heterogeneity (Case 1). There are no large irrigation districts in the upstream reaches of the Yellow River. The observed discharge values at stations TNH and LZ were thus used to validate the model. The discharge at TNH and LZ was well simulated when the precipitation heterogeneity was taken into account. The observed discharge decreased between stations LZ and TDG. Without the irrigation scheme, the simulated discharge increased in the discharge-

decrease zone, although the increase was very small. The decreasing discharge along the main stem of the river was simulated well when irrigation was taken into account. The simulated stream flows were significantly improved with the consideration of both natural and anthropogenic heterogeneities. However, the downstream flows were still overestimated. This suggests that subgrid heterogeneities in precipitation and irrigation in the river basin are significant and likely contribute to the discrepancies between observed and simulated streamflow. Techniques to account for subgrid variability in precipitation and irrigation need to be considered in order to improve stream flow simulations. The results show that annual discharge at station HYK decreased 41% because of irrigation. The anthropogenic influence was prominent downstream from station LZ.

[Figure 7 about here.]

[Figure 8 about here.]

In Figure 9, spatial distributions of water balance components associated with irrigation are shown at a 10×10-km spatial resolution. Figure 9a shows the irrigation water shortage (%) in each grid cell. The irrigation water shortage was calculated from the irrigation water withdrawals to the irrigation water requirements. The water shortage was small in grid cells near the main river stem or inside irrigation districts. Figure 9b gives the irrigation water withdrawal distribution (mm month^{-1}) per unit grid cell area. The largest irrigation water withdrawals occurred in the grid cells in irrigation districts with high irrigation fractions. Figure 9c shows the spatial differences between simulated evaporation with and without the irrigation scheme. Evaporation increased in the irrigation districts and grid cells with high irrigation fractions. Within the simulation period, evaporation averagely increased 25 mm year^{-1} because of irrigation in the Yellow River basin. Runoff spatial differences between simulated evaporation with and without the irrigation scheme are shown in Figure 9d. Total runoff decreased because of irrigation; however, larger runoff occurred in the grid

cells in irrigation districts because a part of flood irrigation becomes return flow and contributes to runoff. Note that all the values in Figure 9 are mean values over their respective grid cells and would have been much larger if reported as values per unit irrigated area.

[Figure 9 about here.]

Figure 10a shows the simulated surface soil wetness (soil moisture to saturated soil moisture) at the top 2-cm soil layer from the ground surface without the irrigation scheme in the Yellow River basin. The surface soil wetness was lower in the upstream area of the river basin where the annual precipitation was small. The surface soil wetness was higher in the lower stream area, which has a semi-humid climate. Figure 10b shows how simulated surface soil wetness changed with the irrigation scheme. The surface soil wetness increased because of irrigation water withdrawals, especially in the irrigation districts and high-irrigation areas. Over the Yellow River basin and the study period, the surface soil wetness increased 5.6% because of irrigation. The surface soil wetness increased 11.2% in the grid cells of the irrigation districts.

[Figure 10 about here.]

The annual average change in the latent heat flux in the Yellow River basin due to irrigation was 2.0 W m^{-2}, or 7.8%, from 1983 to 2000. The latent heat flux increased more in the peak irrigation season from June to August (JJA). The averaged latent heat flux change for the basin was 3.3 W m^{-2} in JJA. Figure 11 shows the peak irrigation season changes in ground surface temperature, canopy temperature, latent heat flux, and sensible heat flux for each grid cell in the Yellow River basin. The ground surface temperature and canopy temperature decreased because of irrigation. The latent heat flux (or evapotranspiration) increased when irrigation was taken into account, while sensible heat flux decreased with irrigation. Again, the largest effects can be seen in cells of the

irrigation districts or for areas with a high percentage of irrigation by area, i.e., the middle and lower reaches of the Yellow River.

Table 3 shows the changes in energy components averaged over the river basin, the grid cells in the irrigation districts, and the grid cells where the irrigation fraction was larger than 30%. Decreases of ground surface temperature and canopy temperature were small over the basin, having values of 0.1 K and 0.06 K, respectively. However, averaged over irrigation districts, irrigation caused ground surface temperature and canopy temperature to decrease by 0.32 K and 0.23 K, respectively. The ground surface temperature and canopy temperature decreased 0.4 K and 0.31 K, respectively, over the grid cells where the irrigation fraction was larger than 30%. The maximum change in ground surface temperature and canopy temperature is shown in a grid cell with an irrigation fraction of 65.5%, where the ground surface temperature and canopy temperature decreased 1.6 K and 1.2 K, respectively. The latent heat flux increases over the grid cells in the irrigation districts and in the grid cells with greater than 30% irrigated area were 11.2 W m^{-2} and 15.5 W m^{-2}, or 3.5 and 4.8 times the average increase over the basin. The maximum change in latent heat flux reached 43.3 W m^{-2}, or 13.3 times the mean value. The sensible heat flux decreases over the grid cells in the irrigation districts and the grid cells with greater than 30% irrigated area were 7.7 W m^{-2} and 10.2 W m^{-2}, or 3.1 and 4.1 times the average decrease over the basin. The maximum change in sensible heat flux reached 37.8 W m^{-2}, or 15.1 times of the mean value. These results indicate that irrigation causes lower surface temperatures, higher evapotranspiration, larger latent heat flux, and smaller sensible heat flux in the Yellow River basin. The lower surface temperatures and higher evapotranspiration resulting from human activities imply that the near-surface atmosphere will be cooler and moister over irrigated areas than over nonirrigated areas.

[Figure 11 about here.]

[Table 3 about here.]

6. Discussions

We evaluated the effects of natural and anthropogenic heterogeneity on hydrological simulation using a distributed biosphere hydrological model (DBHM) system. The model system DBHM is a continuous-time spatially distributed model, integrating hydrological processes and vegetation-atmosphere transfer processes at the river basin scale. It represents the roles of topography, land cover characteristics and human activities in the hydrological cycle with the use of spatially distributed parameters of elevation, land use, land cover, and vegetation condition derived from satellite data, atmospheric forcing from ground observation network, and statistical soil properties and irrigated area from surveys.

The DBHM was used to physically model the relationships of evaporation water demand, soil moisture deficit, and water availability. Precipitation variability was used to evaluate the effect of natural heterogeneity in the hydrological cycle. Runoff simulation could be improved by taking precipitation heterogeneity into account. However, the negative runoff contribution in the semi-arid region could only be simulated by considering anthropogenic heterogeneity. Irrigation water withdrawals were estimated based on the model-predicted soil moisture. The irrigation water was considered to be withdrawn from the river, and no reservoir was included. Because a reservoir could store water for irrigation purposes, the irrigation water withdrawals may have been underestimated. The irrigation scheme gave priority to the upstream area. That is, upstream areas could extract river water without considering the needs of downstream areas. This does not agree with the integrated water management in the Yellow River basin, which is based on water allocation rules along the river main stem. The irrigation scheme assumed that irrigation water was extracted from

the river and used for crops. The direct use of groundwater was not considered because of data unavailability. Localized water use and water waste such as water consumption from an endoric lake were also not taken into account. However, our results indicate that the method yields a reasonable approximation of the overall impact of irrigation in terms of the behavior of the hydrological system.

As this study has shown, both natural and anthropogenic heterogeneities are important factors in hydrological simulations. Precipitation variability and anthropogenic irrigation affect large-scale distributed hydrological patterns in different ways. Runoff, especially surface runoff, will increase over the whole river basin when considering the precipitation variability within grid cells. Anthropogenic heterogeneity caused by irrigation processes will increase evaporation and possibly induce negative runoff in intensively cultivated areas. The effects of anthropogenic heterogeneity are localized, centralized, and related to the intensity of human activities.

Acknowledgement This study was funded by the Ministry of Education, Culture, Sports, Science and Technology (MEXT) of Japan. The work was also partly supported by project 50579031 of the National Natural Science Foundation of China (NSFC). Parts of this study were also supported by Core Research for Evolutional Science and Technology (CREST), the Japan Science and Technology Corporation (JST), the Research Institute for Humanity and Nature (RIHN), and Global Environment Research Fund (GERF) of the Ministry of the Environment of Japan.

References

Acrement, G. J. and V. R. Schneider, 1989: *Guide for Selecting Roughness Coefficients of Natural Channels and Flood Plains*. U.S. Geological Survey Water-Supply Paper 2339. Washington, DC: U.S. Government Printing Office.

Allen, R. G., L. S. Pereira, D. Raes, and M. Smith, 1998: *Crop Evapotranspiration: Guidelines for Computing Crop Water Requirements*. FAO Irrig. and Drain. Paper 56, FAO, Rome.

Angström, A., 1924: Solar and terrestrial radiation. *Q. J. R. Meteorol. Soc.*, **50**, 121–126.

Avissar, R. and R. A. Pielke, 1989: A parameterization of heterogeneous land surfaces for atmospheric numerical models and its impact on regional meteorology. *Mon. Weather Rev.*, **117**, 2113–2136.

Avissar, R. and T. Schmidt, 1998: An evaluation of the scale at which ground-surface heat flux patchiness affects the convective boundary layer using large-eddy simulations. *J. Atmos. Sci.*, **55**, 2666–2689.

Boucher, O., G. Myhre, and A. Myhre, 2004: Direct human influence of irrigation on atmospheric water vapour and climate. *Clim. Dyn.*, **22**, 597–603.

Cesaraccio, C., D. Spano, P. Duce, and R. L. Snyder, 2001: An improved model for determining degree-day values from daily temperature data. *Int. J. Biometeorol.*, **45**, 161–169.

Chen, J. Y., C. Y. Tang, Y. Sakura, A. Kondoh, and Y. J. Shen, 2002: Groundwater flow and geochemistry in the lower reaches of the Yellow River: a case study in Shandang Province, China. *Hydrogeol. J.*, **10**, 587–599.

Childs, E. C., 1971: Drainage of groundwater resting on a sloping bed. *Water Resour. Res.*, **7**, 1256–1263.

Chow, V. T., 1959: *Open-channel Hydraulics*. McGraw-Hill: New York.

Cosby, B. J., G. M. Hornberger, R. B. Clapp, and T. R. Ginn, 1984: A statistical exploration of the relationships of soil moisture characteristics to the physical properties of soils. *Water Resour. Res.*, **20**, 682–690.

Desborough, C. E. and A. J. Pitman, 1998: The BASE land surface model. *Global Planet. Change*, **19**, 3–181.

Dickinson, R. E., A. Henderson-Sellers, P. J. Kennedy, and M. F. Wilson, 1986: *Biosphere-atmosphere transfer scheme (BATS) for the NCAR community climate model*. NCAR Tech. Note NCAR/TN-387+STR, National Center for Atmospheric Research, Boulder, CO.

Döll, P. and S. Siebert, 2002: Global modeling of irrigation water requirements. *Water Resour. Res.*, **38**, 8.1–8.10, doi:10.1029/2001WR000355.

Doorenbos, J. and W. O. Pruitt, 1977: *Guidelines for predicting crop water requirements*. FAO Irrig. and Drain. Paper 24, FAO, Rome, 156 pp.

Entekhabi, D. and P. S. Eagleson, 1989: Land surface hydrology parameterization for atmospheric general circulation models including subgrid scale spatial variability. *J. Clim.*, **2**, 816–831.

FAO, 1995: Digital Soil Map of the World and Derived Soil Properties. CD-ROM, Land and Water Digital Media Series No. 7, Food and Agriculture Organization of the United Nations, Rome.

Feng, J. M., T. Wang, S. Z. Qi, and G. W. Xie, 2005: Land degradation in the source region of the

Yellow River, northeast Qinghai-Xizang Plateau: classification and evaluation. *Environ. Geol.*, **47**, 459–466.

Fu, G., S. L. Chen, C. M. Liu, and D. Shepard, 2004: Hydro-climatic trends of the Yellow River basin for the last 50 years. *Climatic Change*, **65**, 149–178.

Gao, X. and S. Sorooshian, 1994: A stochastic precipitation disaggregation scheme for GCM applications. *J. Clim.*, **7**, 238–247.

Ghan, S. J., J. C. Liljegren, W. J. Shaw, J. H. Hubbe, and J. C. Doran, 1997: Influence of subgrid variability on surface hydrology. *J. Clim.*, **10**, 3157–3166.

Giorgi, F., 1997a: An approach for the representation of surface heterogeneity in land surface models. Part I: theoretical framework. *Mon. Weather Rev.*, **125**, 1885–1899.

— 1997b: An approach for the representation of surface heterogeneity in land surface models. Part II: validation and sensitivity experiments. *Mon. Weather Rev.*, **125**, 1900–1919.

Giorgi, F. and R. Avissar, 1997: Representation of heterogeneity effects in Earth system modeling: experience from land surface modeling. *Rev. Geophys.*, **35**, 413–438.

Gordon, L. J., W. Steffen, B. F. Jonsson, C. Folke, M. Falkenmark, and A. Johannessen, 2005: Human modification of global water vapor flows from the land surface. *Proc. Natl. Acad. Sci. U. S. A.*, **102**, 7612–7617.

Haddeland, I., D. P. Lettenmaier, and T. Skaugen, 2005: Effects of irrigation on the water and energy balances of the Colorado and Mekong river basins. *J. Hydrol.*, **324**, 210–223, doi:10.1016/j.jhydrol.2005.09.028.

Hager, W. H., 1984: A simplified hydrological rainfall-runoff model. *J. Hydrol.*, **74**, 151–170.

Koster, R. D. and M. J. Suarez, 1992a: A comparative analysis of two land surface heterogeneity representations. *J. Clim.*, **5**, 1379–1390.

— 1992b: Modeling the land surface boundary in climate models as a composite of independent vegetation stands. *J. Geophys. Res.*, **97**, 2697–2715.

Leung, L. R. and S. J. Ghan, 1998: Parameterizing subgrid orographic precipitation and surface cover in climate models. *Mon. Weather Rev.*, **126**, 3271–3291.

Li, C., D. Yang, G. Ni, and H. Hu, 2004: Simulation of irrigation water consumption in the Yellow River basin using a distributed hydrological model. *Proceedings of the Second International Conference on Hydrology and Water Resources in Asia Pacific Region*, APHW, Singapore.

Liang, X., D. P. Lettenmaier, and E. F. Wood, 1996: One-dimensional statistical dynamic representation of subgrid spatial variability of precipitation in the two-layer variable infiltration capacity model. *J. Geophys. Res.*, **101**, 21403–21422, doi:10.1029/96JD01448.

Liang, X. and Z. Xie, 2001: A new surface runoff parameterization with subgrid-scale soil heterogeneity for land surface models. *Adv. Water Resour.*, **24**, 1173–1193.

Lighthill, M. H. and G. B. Whitham, 1955: On kinematic waves, I. Flood movement in long rivers. *Proc. R. Soc. London*, **229**, 281–316.

Liu, C. M. and S. F. Zhang, 2002: Drying up of the Yellow River: its impacts and counter-measures. *Mitigation and Adaptation Strategies for Global Change*, **7**, 203–214.

Liu, C. M. and H. X. Zheng, 2004: Changes in components of the hydrological cycle in the Yellow River basin during the second half of the 20th century. *Hydrol. Process.*, **18**, 2337–2345.

Loveland, T. R., B. C. Reed, J. F. Brown, D. O. Ohlen, Z. Zhu, L. Yang, and J. W. Merchant, 2000: Development of a global land cover characteristics database and IGBP DISCover from 1 km AVHRR data. *Int. J. Remote Sens.*, **21**, 1303–1330.

Manabe, S., 1969: Climate and the ocean circulation I. The atmospheric circulation and the hydrology of the Earth's surface. *Mon. Weather Rev.*, **97**, 739–774.

Milly, P. C. D. and P. S. Eagleson, 1988: Effect of storm scale on surface runoff volume. *Water Resour. Res.*, **24**, 620–624.

Murphy, A. H., 1988: Skill scores based on the mean square error and their relationships to the correlation coefficient. *Mon. Weather Rev.*, **16**, 2417–2424.

Myneni, R. B., R. R. Nemani, and S. W. Running, 1997: Estimation of global leaf area index and absorbed par using radiative transfer models. *IEEE T Geosci. Remote.*, **35**, 1380–1393.

New, M., M. Hulme, and P. Jones, 2000: Representing twentieth-century space-time climate variability. Part II: development of 1901-96 monthly grids of terrestrial surface climate. *J. Clim.*, **13**, 2217–2238.

Pfafstetter, O., 1989: Classification of hydrographic basins: coding methodology. unpublished manuscript, Departamento Nacional de Obras de Saneamento, 18 August 1989, Rio de Janeiro.

Pitman, A. J., A. Henderson-Sellers, and Z. L. Yang, 1990: Sensitivity of regional climates to localised precipitation in global models. *Nature*, **346**, 734–737.

Revfeim, K. J. A., 1997: On the relationship between radiation and mean daily sunshine. *Agr. Forest Meteorol.*, **86**, 181–191.

Sellers, P. J., Y. Mintz, Y. C. Sud, and A. Dalcher, 1986: A simple biosphere model (SiB) for use within general circulation models. *J. Atmos. Sci.*, **43**, 505–531.

Sellers, P. J., D. A. Randall, G. J. Collatz, J. A. Berry, C. B. Field, D. A. Dazlich, C. Zhang, G. D. Collelo, and L. Bounoua, 1996: A revised land surface parameterization (SiB2) for atmospheric GCMs - Part I: model formulation. *J. Clim.*, **9**, 676–705.

Seth, A. and F. Giorgi, 1996: Three-dimensional model study of organized mesoscale circulations induced by vegetation. *J. Geophys. Res.*, **101**, 7371–7392.

Seth, A., F. Giorgi, and R. E. Dickinson, 1994: Simulating fluxes from heterogeneous land surfaces: explicit subgrid method employing the biosphere-atmosphere transfer scheme (BATS). *J. Geophys. Res.*, **99**, 18651–18667.

Siebert, S., P. Döll, S. Feick, and J. Hoogeveen, 2005: *Global Map of Irrigated Areas Version 3.0*. Johann Wolfgang Goethe University, Frankfurt am Main, Germany/FAO, Rome, Italy.

Tang, Q., T. Oki, and H. Hu, 2006: A distributed biosphere hydrological model (DBHM) for large river basin. *Ann. J. Hydraul. Eng. JSCE*, **50**, 37–42.

Towner, G. D., 1975: Drainage of groundwater resting on a sloping bed with uniform rainfall. *Water Resour. Res.*, **11**, 144–147.

Verdin, K. L. and J. P. Verdin, 1999: A topological system for delineation and codification of the Earth's river basins. *J. Hydrol.*, **218**, 1–12.

Xia, J., Z. G. Wang, G. S. Wang, and G. Tan, 2004: The renewability of water resources and its quantification in the Yellow River basin, China. *Hydrol. Process.*, **18**, 2327–2336.

Xu, J. X., 2005: The water fluxes of the Yellow River to the sea in the past 50 years, in response to climate change and human activities. *Hydrol. Process.*, **35**, 620–631.

Xu, Z. X., K. Takeuchi, H. Ishidaira, and X. W. Zhang, 2002: Sustainability analysis for Yellow River water resources using the system dynamics approach. *Water Resour. Manag.*, **16**, 239–261.

Yang, D. W., C. Li, H. P. Hu, Z. D. Lei, S. X. Yang, T. Kusuda, T. Koike, and K. Musiake, 2004: Analysis of water resources variability in the Yellow River of China during the last half century using historical data. *Water Resour. Res.*, **40**, W06502, doi:10.1029/2003WR002763.

Yang, K., G. W. Huang, and N. Tamai, 2001: A hybrid model for estimating global solar radiation. *Sol. Energy*, **70**, 13–22.

Yang, K. and T. Koike, 2005: A general model to estimate hourly and daily solar radiation for hydrological studies. *Water Resour. Res.*, **41**, doi:10.1029/2005WR003976.

Yeh, P. J. F. and E. A. B. Eltahir, 2005: Representation of water table dynamics in a land surface scheme. Part II: subgrid variability. *J. Clim.*, **18**, 1881–1901.

Zeng, X. M., M. Zhao, B. K. Su, J. P. Tang, Y. Q. Zheng, Y. J. Zhang, and J. Chen, 2002: Effects of subgrid heterogeneities in soil infiltration capacity and precipitation on regional climate: a sensitivity study. *Theor. Appl. Climatol.*, **73**, 207–221.

List of Figures

1 The DBHM model. 31

2 Precipitation area-amount relationships. 32

3 The Yellow River basin (the hydrologic gauges are marked with abbreviation in brackets). 33

4 (a) Mean annual precipitation from 1983 to 2000 and (b) irrigated area (%) in the Yellow River basin. 34

5 Simulated and observed mean monthly stream flow at Tangnaihai station from 1983 to 2000. 35

6 Simulated and observed daily stream flow at Tangnaihai station. 36

7 Effects of precipitation heterogeneity on total runoff and subsurface runoff simulations from 1983 to 2000 in the Yellow River Basin. 37

8 Effects of natural and anthropogenic heterogeneities on annual stream flow along the Yellow River from upstream to downstream. 38

9 Spatial effects of irrigation on water balance components in the Yellow River basin; (a) water shortage in a grid cell with an irrigated area, (b) irrigation water withdrawal, (c) evaporation change, (d) runoff change. 39

10 (a) Simulated surface soil wetness (top 2 cm) without irrigation in the Yellow River basin; (b) simulated surface soil wetness change (%) with irrigation. 40

11 Spatial effects of irrigation on energy balance components (a) changes in ground surface temperature dT_g, (b) changes in canopy temperature dT_c, (c) changes in latent heat fluxes $raet$, and (d) changes in sensible heat fluxes $raht$ in the peak irrigation season (JJA). 41

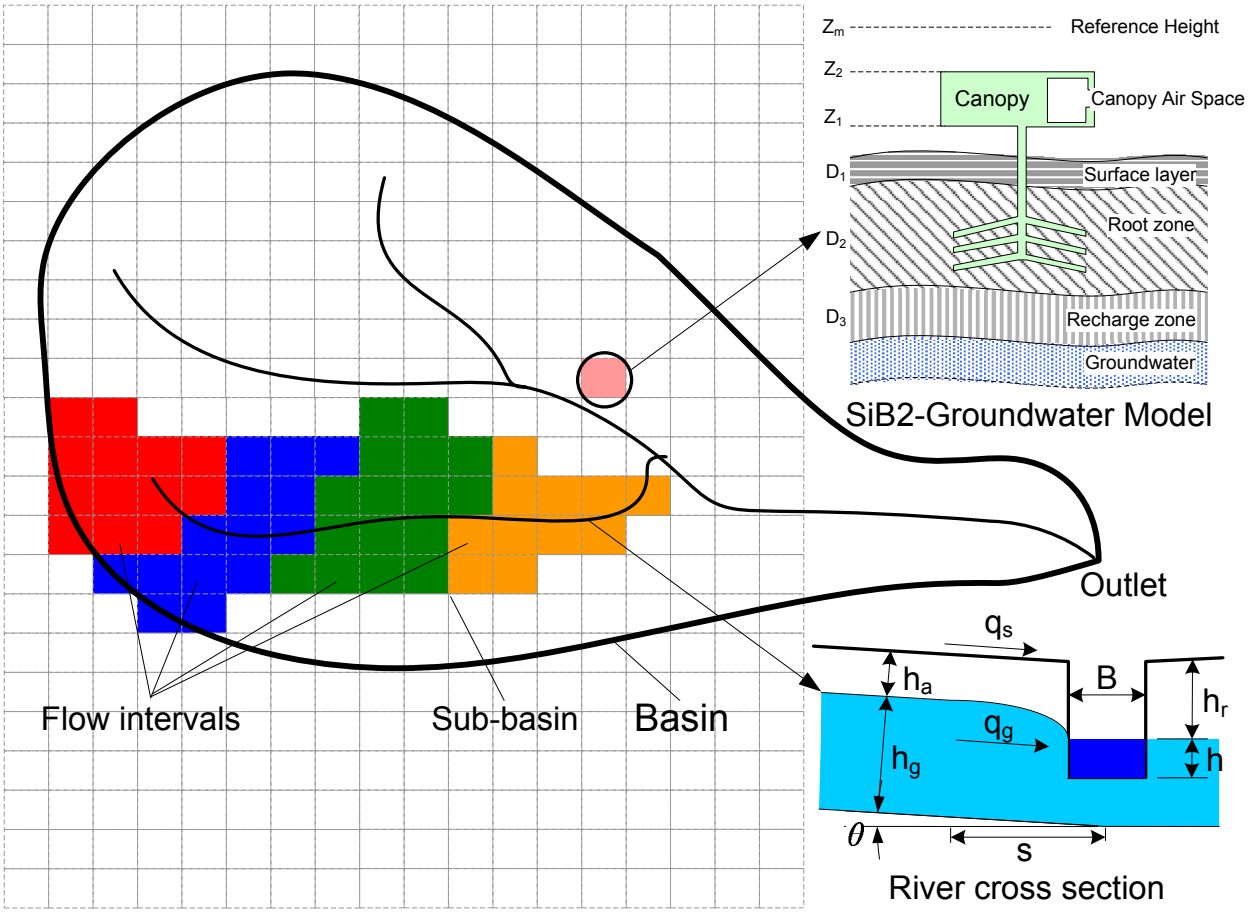

Figure 1: The DBHM model.

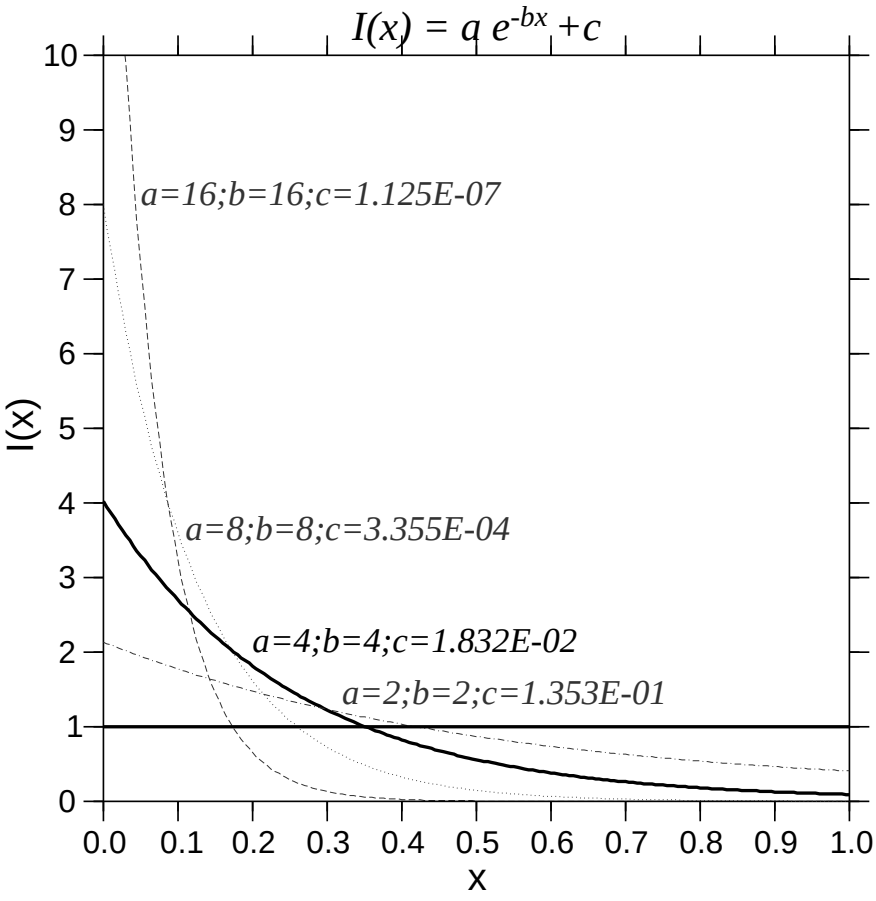

Figure 2: Precipitation area-amount relationships.

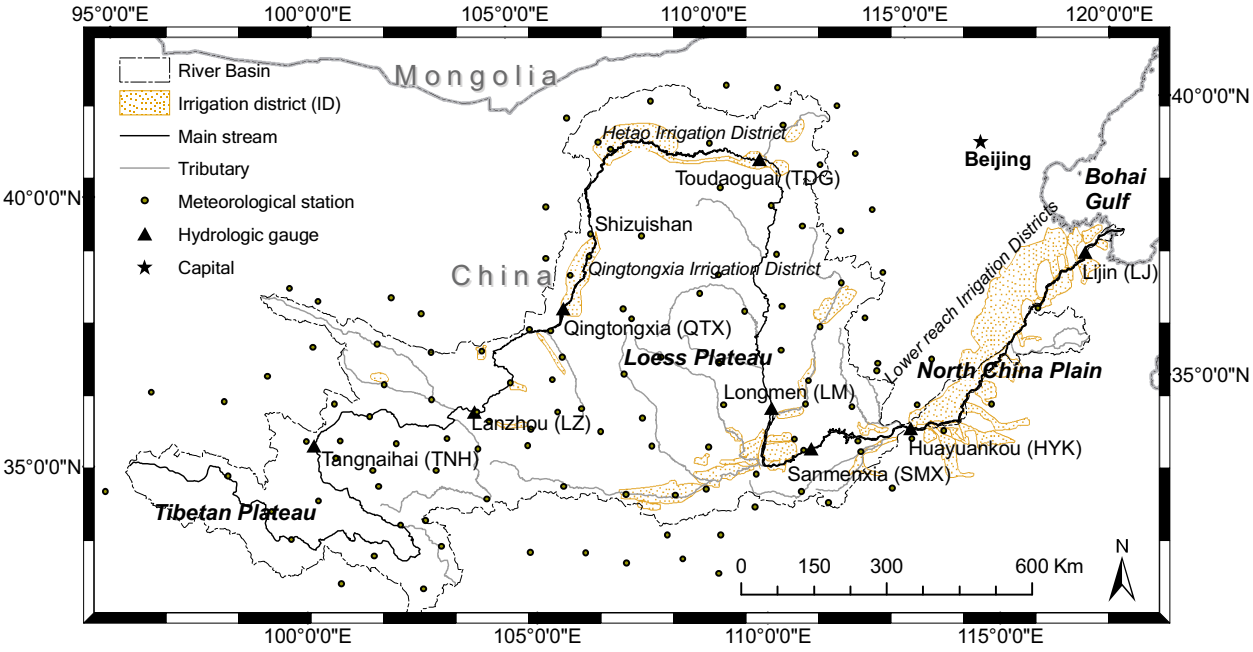

Figure 3: The Yellow River basin (the hydrologic gauges are marked with abbreviation in brackets).

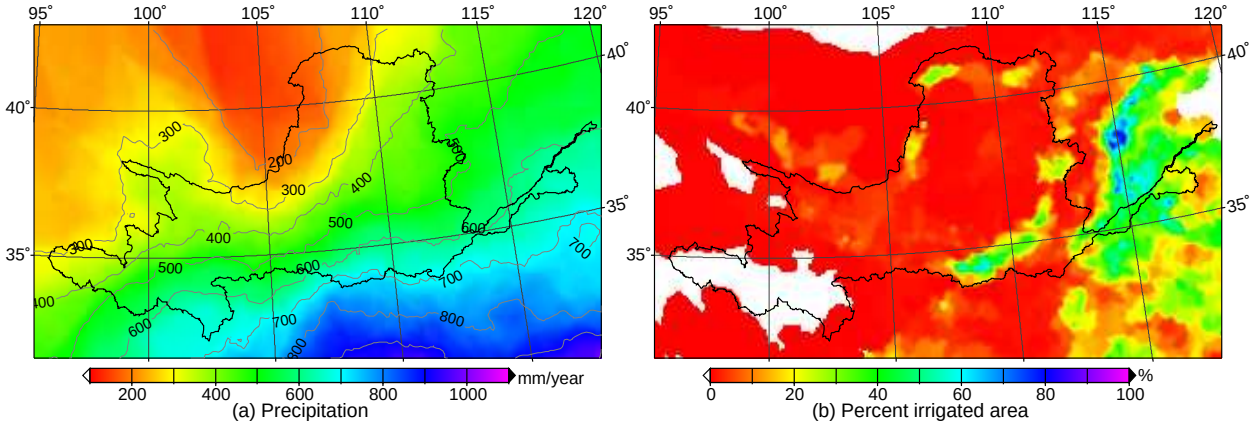

Figure 4: (a) Mean annual precipitation from 1983 to 2000 and (b) irrigated area (%) in the Yellow River basin.

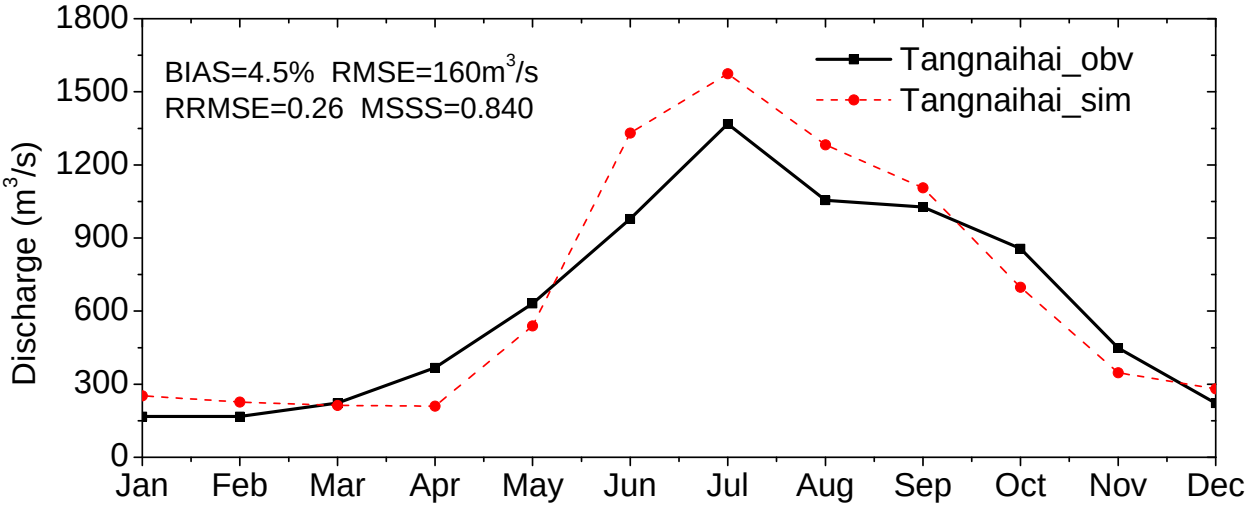

Figure 5: Simulated and observed mean monthly stream flow at Tangnaihai station from 1983 to 2000.

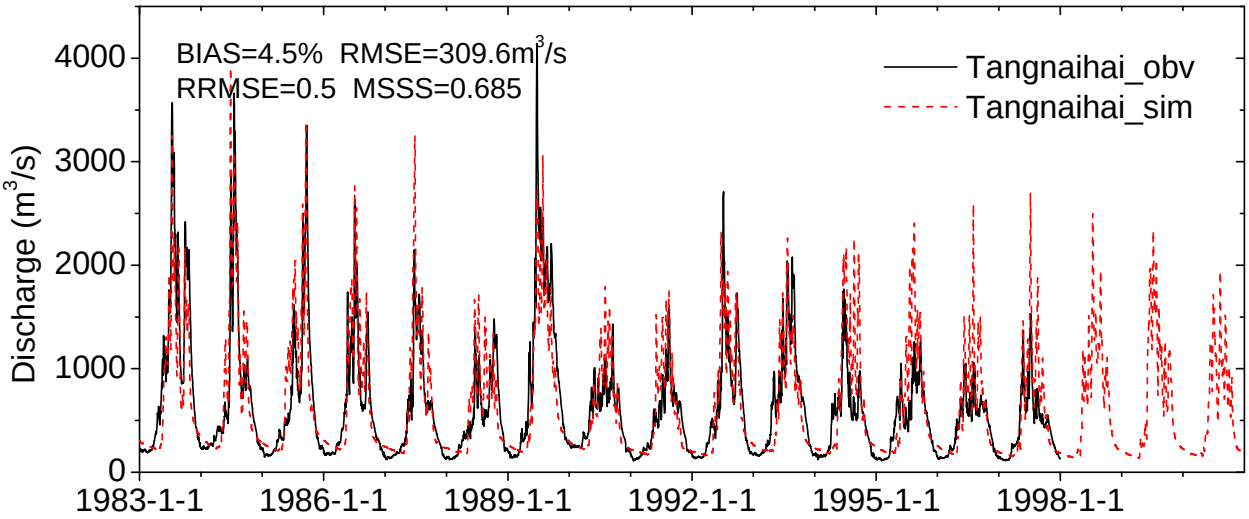

Figure 6: Simulated and observed daily stream flow at Tangnaihai station.

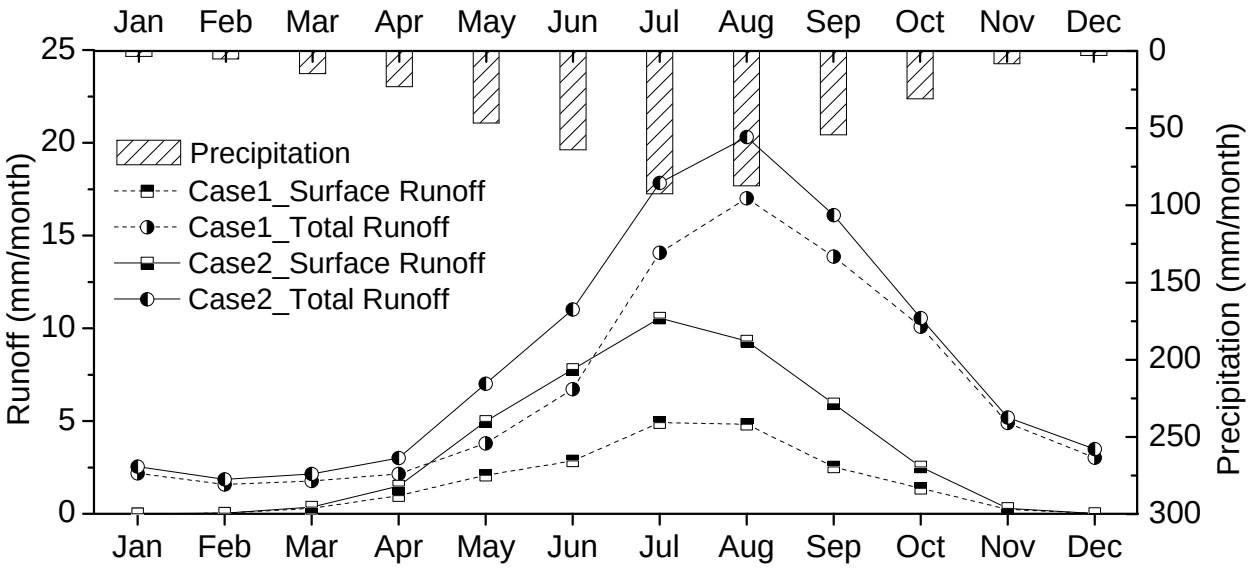

Figure 7: Effects of precipitation heterogeneity on total runoff and subsurface runoff simulations from 1983 to 2000 in the Yellow River Basin.

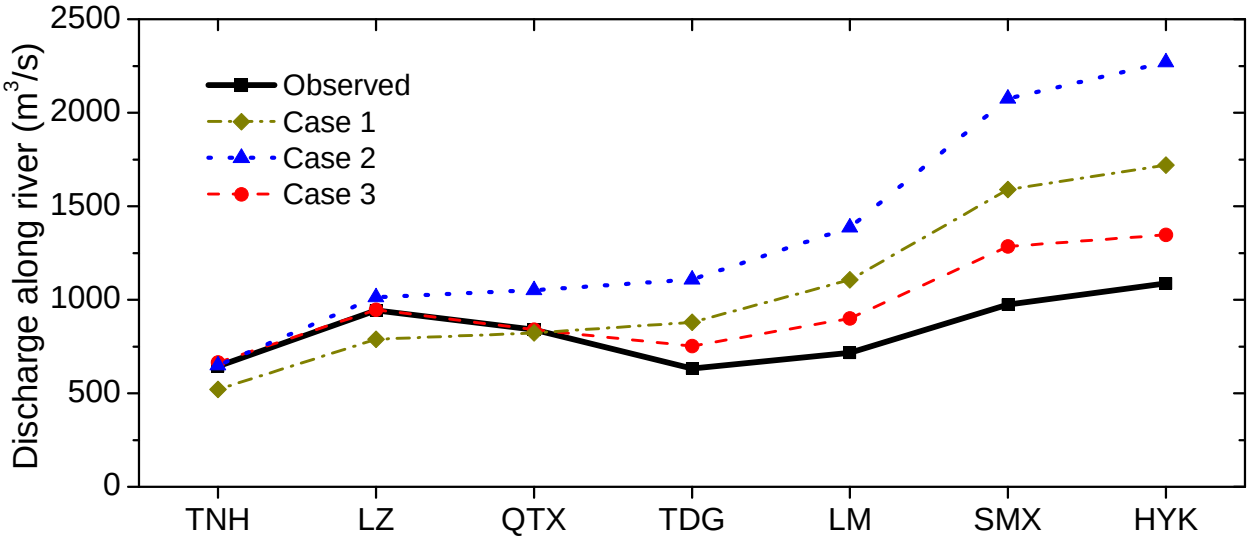

Figure 8: Effects of natural and anthropogenic heterogeneities on annual stream flow along the Yellow River from upstream to downstream.

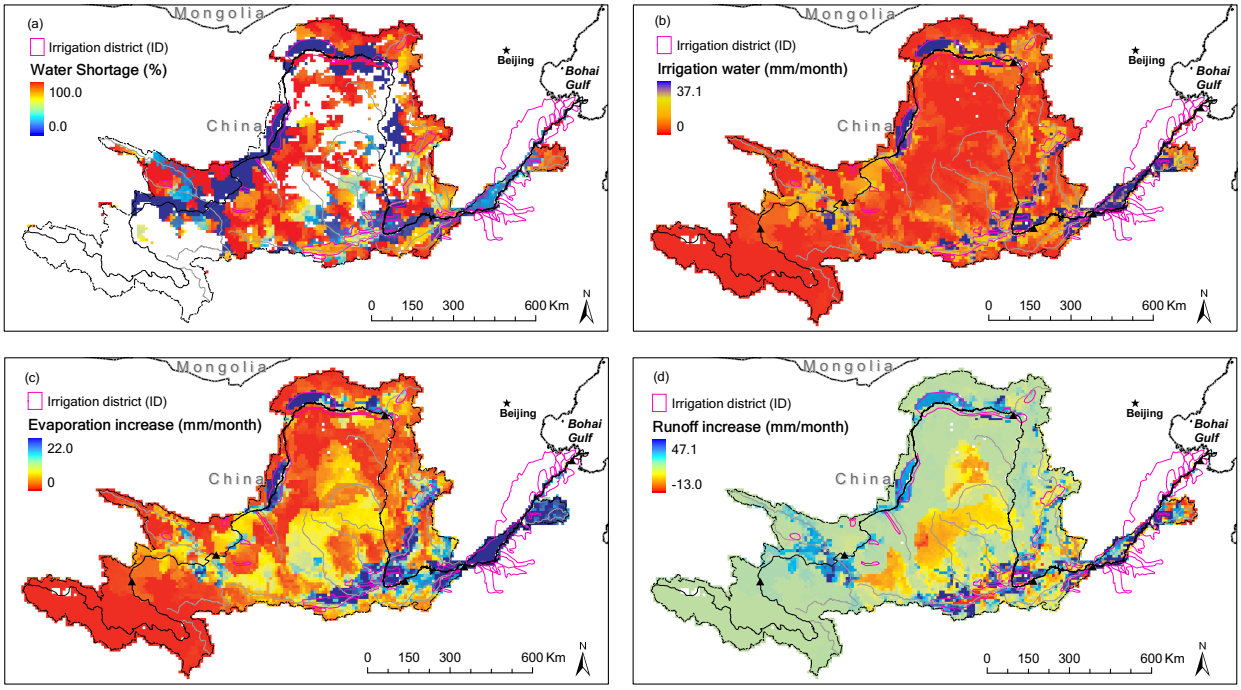

Figure 9: Spatial effects of irrigation on water balance components in the Yellow River basin; (a) water shortage in a grid cell with an irrigated area, (b) irrigation water withdrawal, (c) evaporation change, (d) runoff change.

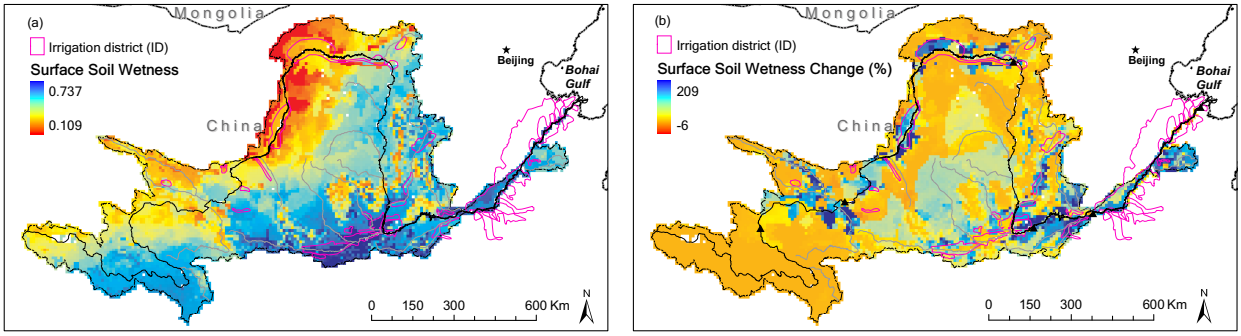

Figure 10: (a) Simulated surface soil wetness (top 2 cm) without irrigation in the Yellow River basin; (b) simulated surface soil wetness change (%) with irrigation.

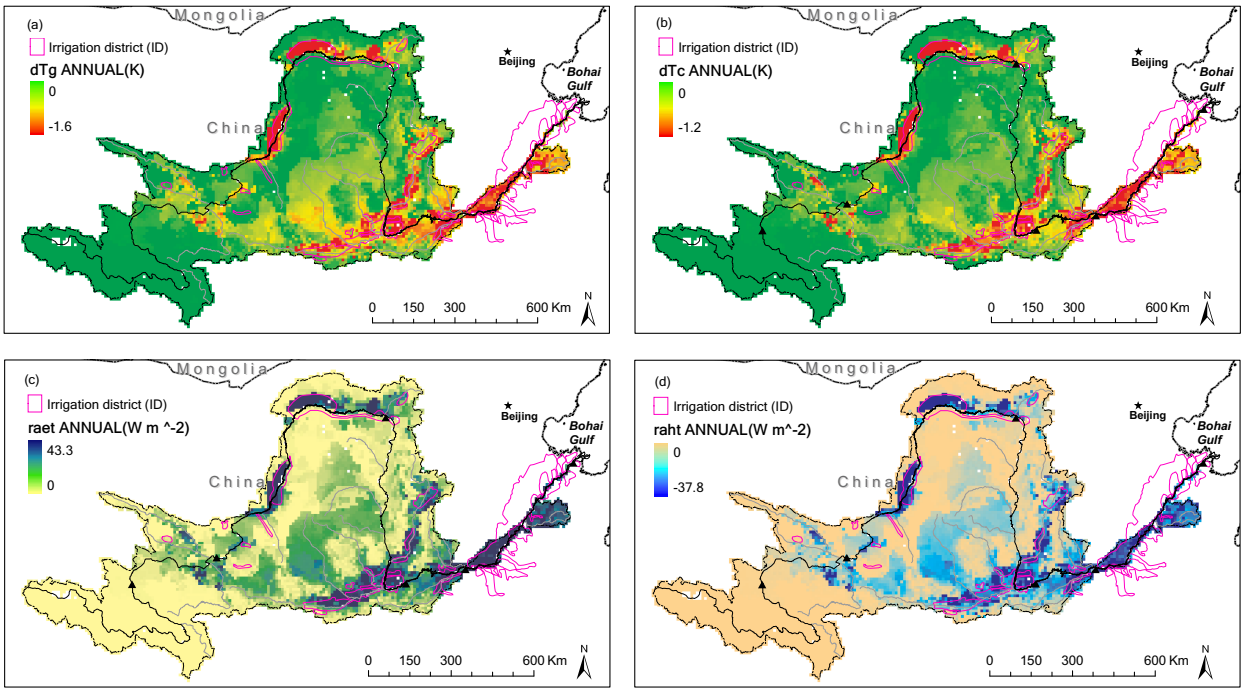

Figure 11: Spatial effects of irrigation on energy balance components (a) changes in ground surface temperature dT_g, (b) changes in canopy temperature dT_c, (c) changes in latent heat fluxes $raet$, and (d) changes in sensible heat fluxes $raht$ in the peak irrigation season (JJA).

List of Tables

1 Simulated and reported annual irrigation water consumption ($10^9 m^3$) 43

2 Mean annual runoff (R), evaporation (E) for the various case from 1983 to 2000 (mm $year^{-1}$) 44

3 Changes in energy components in peak irrigation season JJA 45

Table 1: Simulated and reported annual irrigation water consumption ($10^9 m^3$)

Time period	Upper reaches[a]	Middle reaches	Lower reaches	Total
1980-1989 (reported)	12.11	6.21	11.29	29.61
1983-1989 (simulated)	8.15	7.90	11.06	27.11
1990-1995 (reported)	13.17	6.02	10.78	29.96
1990-1995 (simulated)	6.88	7.98	9.63	24.49

[a]The effect of an endoric lake was not considered in the simulations.

Table 2: Mean annual runoff (R), evaporation (E) for the various case from 1983 to 2000 (mm year^{-1})

Subdivisions	Precipitation	Observed		case 1		case 2		case 3	
		R	E	R	E	R	E	R	E
Up TNH	483	173	310	140	344	174	309	178	305
TNH-LZ	416	88	327	79	336	108	307	83	332
LZ-QTX	316	-61	377	21	295	22	294	-63	379
QTX-TDG	240	-56	296	15	225	15	225	-23	264
TDG-LM	395	18	377	50	345	61	334	32	363
LM-SMX	523	42	481	80	443	114	409	64	459
SMX-HYK	601	86	515	97	504	144	457	46	555

Table 3: Changes in energy components in peak irrigation season JJA

Item	Avg.	ID[a]	IF[b]	Max.	Min.
Ground surface temperature dT_g (K)	-0.1	-0.32	-0.4	0.0	-1.6
Canopy temperature dT_c (K)	-0.06	-0.23	-0.31	0.0	-1.2
Latent heat fluxes $raet$ (W m^{-2})	3.3	11.2	15.5	43.3	0.0
Sensible heat fluxes $raht$ (W m^{-2})	-2.5	-7.7	-10.2	0.0	-37.8

[a] Averaged for the irrigation district grid cells.
[b] Averaged for grid cells in which the irrigation fraction is larger than 30%.